

Dislocation glide driven interstitial shuffling of oxygen interstitials in titanium

Eric Rothchild ¹, Max Poschmann ², M. Asta ¹ and D. C. Chrzan ¹

¹*Department of Materials Science and Engineering, University of California, Berkeley, California 94720, USA*

²*Faculty of Energy Systems and Nuclear Science, Ontario Tech University, Oshawa, Ontario, Canada L1H 7K4*



(Received 12 June 2022; accepted 18 August 2022; published 2 September 2022)

The bypassing of an oxygen interstitial by $\langle a \rangle$ -type screw dislocations in Ti is studied as a function of the dislocation core structure using an empirical potential and the nudged elastic band method. It is shown that an interstitial oxygen will be pushed from the octahedral site into a new interstitial site in the dislocation core. From there, with the passage of a dislocation spread primarily on the prismatic plane there is a high energy barrier for oxygen to return to the octahedral site. Instead, it is likely to shuffle into the neighboring hexahedral site, a transition expected to lead to slip plane softening. For dislocations spread primarily within the pyramidal planes, the octahedral to hexahedral transition is much less likely as there is little to no barrier for the oxygen to return to the original octahedral site. This difference in barriers is then explained by a reduction in the attraction between the hexahedral site and the dislocation core, calculated within micromechanics, as the core transitions from a prismatic to a pyramidal state.

DOI: [10.1103/PhysRevMaterials.6.093601](https://doi.org/10.1103/PhysRevMaterials.6.093601)

I. INTRODUCTION

Titanium alloys offer a desirable combination of corrosion resistance, high strength to weight ratio, and high formability, yet their use is limited by high cost compared to alternative materials [1]. This high cost is partially due to the strict requirements of interstitial content in the production and manufacturing process. Oxygen interstitial impurities, in particular, cause a dramatic strength increase in α -titanium but adversely impact the ductility and fracture toughness [2,3].

The profound strengthening by interstitial oxygen has been explained as a contact interaction with the dislocation core [4]. The lowest energy site for oxygen impurities in α -titanium is the octahedral interstitial site; however, this site is effectively eliminated in the core of an $\langle a \rangle$ -type dislocation. This creates a strong but short-range repulsion between the interstitial atom and the dislocation, as the passing dislocation pushes the oxygen atom into an interstitial site specific to the dislocation core, henceforth referred to as the core site.

It has been shown that the decrease in ductility in Ti alloys is correlated with a wavy-to-planar slip transition of the $\langle a \rangle$ -type screw dislocation [5,6]. A wavy-to-planar transition of this sort is often seen in alloys with short-range order, as the destruction of the short-range order is responsible for a slip-plane softening effect [7,8]. In the case of oxygen in titanium, this has been ruled out as a sufficient source of slip-plane softening [5].

More recently, it was suggested that slip-plane softening is a result of dislocation glide driven shuffling of oxygen from the octahedral (Oct) interstitial site to the higher energy hexahedral (Hex) interstitial site, where it presents a weaker obstacle to dislocation glide [5]. This hypothesis was supported by experimental trends, as well as generalized stacking fault (GSF) calculations. GSF calculations show that passage

of dislocation might lead to shuffling of the oxygen interstitials and that this shuffling will weaken the slip plane. However, the distortion associated with a dislocation differs substantially from that of the GSF, and there are many possible ways to handle the degrees of freedom and starting positions of an interstitial atom in a GSF calculation that can lead to different conclusions. Hence, there is a need to examine directly the shuffling of interstitials during dislocation glide.

The potential for polymorphism of dislocation cores could strongly influence the dynamics of $\langle a \rangle$ -type dislocations in α -Ti. Clouet *et al.* used density functional theory (DFT) to compute the dislocation core structures and, using the nudged elastic band (NEB) method, Peierls barriers for dislocations slipping on the prismatic and pyramidal planes in both α -Ti and Zr [9]. They concluded that the observed “jerky” motion of dislocations in α -Ti crystals arises from the fact that a dislocation with its core spread on the pyramidal planes cannot glide on the prismatic plane until the core is reconfigured to be spread on the prismatic plane. The energy barrier to reconfiguring is larger than the energy barrier for prismatic glide once the dislocation is in the prismatic spread configuration. The result is a type of locking-unlocking motion, as is observed using TEM. In contrast, for Zr, the dislocation cores are always predicted to be spread on the prismatic plane and, consequently, display smooth glide.

In addition, DFT-based total energy calculations of the properties of periodic arrays of dislocations have shown that the low energy pyramidal configuration is of the order of 20 meV/ b more favorable than the prismatic configuration [9–11], with b being the magnitude of the Burgers vector. It was recently argued that the predicted small energy differences between differing dislocation core morphologies will lead to temperature driven core structure fluctuations [12,13].

Hence, it is essential to consider the effects of differing core morphologies on the expected shuffling probability.

In this study, dislocation glide driven interstitial shuffling is studied in α -Ti using an empirical modified embedded atom method (MEAM) potential [14]. Specifically, simulations of full dislocations passing through interstitial atoms while slipping prismatically are presented. With this MEAM potential, the prismatic core is favored over the pyramidal one, a reverse of the DFT prediction. However, applying an appropriate non-Schmid stress enables tuning of the relative energies of the competing core structures [15]. Here, NEB simulations are performed for the case of no non-Schmid stress, i.e., with a prism-dissociated core, and under 3 GPa of non-Schmid stress, where the pyramidal core is most stable (at zero temperature). The simulations suggest that interstitial shuffling is likely when the prismatic core is favored and unlikely when the pyramidal core is favored. For the purposes of this study, NEB calculations are preferable to molecular dynamics (MD) simulations as the high strain rates necessarily used in MD can lead to behaviors that are not relevant at lower strain rates. However, the results of MD simulations presented in the Appendix are consistent with the predictions of NEB calculations.

Additionally, the interaction energy between the interstitial sites and strain fields around the dislocation core are calculated with a micromechanical model. This model shows an attractive elastic interaction between the dislocation and interstitial oxygen along the prismatic direction. The attractive interaction between the hexahedral oxygen and the dislocation core is stronger for the prismatically spread core than the pyramidally spread one, which is an explanation of the increased propensity for shuffling in the prismatic case.

II. METHODS

A. NEB simulations

Dislocation dipoles were placed into supercells using Daw's solution for a periodic array of dislocations [16], with a deformation applied to the whole supercell to account for the distortion of the dislocations as prescribed by Lehto and Öberg [17]. With one dislocation in a constant position, the other was placed at sites ranging from $2c$ to the left to $2c$ to the right of the interstitial atom, where c is the height of the unit cell. (There is a local minimum in the energy for motion by $c/2$ stemming from the symmetry of the hcp structure.) These cells were dislocation quadrupoles with two dislocations per cell, described as an O arrangement [18]. Each cell was 32 [0001] by 16 [1 $\bar{1}$ 01] and either $3b$, $15b$, $30b$, or $60b$ deep, with the Burger's vector b being $\frac{1}{3}\langle 11\bar{2}0 \rangle$. For simulations including oxygen atoms, there was an octahedral or hexahedral interstitial oxygen placed in the prismatic glide plane adjacent to one of the two dislocations in the cell (as shown in Fig. 1).

All energy calculations and NEB simulations were performed using LAMMPS [19–23]. First, the cells were relaxed using conjugate gradient minimization. Due to the variety of possible core structures, the exact placement of the dislocation core affected the energy of the initial relaxation, so many trials with slightly varied initial positions were considered. Linear

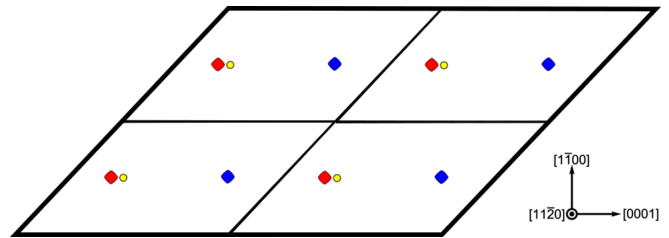


FIG. 1. A diagram of quadrupole-arranged dislocations used for the NEB simulations. Red and blue diamonds mark dislocations with opposite signs before prismatic displacement. A yellow circle marks the position of the oxygen. When the left dislocation has slipped on top of the oxygen, by moving $2c$, the arrangement is perfectly quadrupolar.

interpolations of the lowest energy results of the above relaxations were used as starting points for the NEB calculations.

NEB simulations were performed in two stages. The first stage included nine images, starting from the linear interpolation of the initial relaxations. Several cases were considered: no oxygen, oxygen in the Hex site throughout, oxygen starting in the Oct site and ending in the Hex site, and oxygen starting and ending in the Oct site. In the simulations for cells $3b$ deep with the oxygen atom starting and ending in the Oct site, it was found that the oxygen slipped into the Hex site halfway through the eight slip events, before returning to the original site. In order to get calculations to converge for the Oct \rightarrow Oct case in cells deeper than $3b$, it was necessary to have an initial pathway with the oxygen atom in the Hex site halfway through the path.

The second stage used, as a starting configuration for the NEB calculation, 41 images linearly interpolated between the nine-image pathway determined in the first stage. All NEB calculations were converged to a minimum force of 1.6×10^{-6} eV/Å per atom using fire minimization. For this process the NEB force with a spring constant of 1 eV/Å was applied only to atoms within a 15 Å circular region around the dislocation at the midpoint of the slip events. It has been suggested that limiting the number of atoms the NEB force is applied to may lead to more accurate results for Peierls barriers and stresses [24].

As will be shown later, the results of the calculation above have a sharp or discontinuous energy pathway when the octahedral atom moves to or from the core interstitial site. In order to more clearly examine the behavior during the transition back to the octahedral site, a set of calculations using climbing image NEB (CI-NEB) was performed. It used final images from the original 41-image NEB simulation, starting from the Oct \rightarrow Hex path (i.e., where interstitial shuffling has occurred) and ending on the Oct \rightarrow Oct path (where interstitial shuffling has not occurred). These are calculated to be compared with the Oct \rightarrow Hex path described before. If there were a high barrier to return to the octahedral site, a dislocation would be expected to leave hexahedral interstitials in its wake. For most of these calculations, eight images from a linear interpolation of the start and end structures were used. The NEB force was applied to the same atoms as in the first set of NEB calculations; however, the spring constant was increased to 5 eV/Å, and a parallel spring constant of 1 eV/Å was also

applied. For the second return paths under no non-Schmid stress 41 images were used, the first and last of which had a spring constant of $100 \text{ eV}/\text{\AA}$ applied because the first image was not a metastable position and more images were required for convergence of the simulation. Additionally, the spring constant on the middle images was reduced to $1 \text{ eV}/\text{\AA}$.

The position of the dislocation at each point in the NEB was calculated by first evaluating the Nye tensor [25] at each atom using the BABEL software package [26]. Then, the values of the screw component were averaged along the dislocation line direction, and the center of the Burgers vector density was computed (accounting for the periodic boundary conditions [27]). This center is what is referred to as the dislocation position for each of the NEB-determined minimum energy paths.

For comparison of energies between the far field and near-dislocation interstitial atoms, calculations were performed using cells similar to those in the $15b$ case, but with no dislocation present. The cases considered were, once again, the presence of an octahedral interstitial, a hexahedral interstitial, and no oxygen atom.

B. Micromechanics

A micromechanical approach can be used to better understand the origin of the interaction between the interstitial atoms and the dislocations. Within this approach, the elastic interaction energy between an interstitial atom and a strain field may be computed according to [28]

$$E_{\text{int}} = -P_{ij}\epsilon_{ij}(x), \quad (1)$$

where \mathbf{P} is the elastic dipole tensor of the interstitial atom at position x and $\epsilon(x)$ is the strain at position x produced by the dislocation.

The elastic dipole tensors for hexahedral and octahedral oxygen in the MEAM potential were calculated using the Kanzaki method by Poschmann [29,30]. In this method, the elastic dipole tensor was calculated using the forces on atoms calculated by LAMMPS to determine the Kanzaki force \mathbf{f} [30]. This was done by relaxing the atomic positions with the interstitial, then removing it and finding the resulting force: this force is the negative of the Kanzaki force. The elastic dipole tensor is then

$$P_{ij} = \sum_{k=1}^N (r_i^k - r_i^{\text{interstitial}}) f_j^k \quad (2)$$

where the sum is over noninterstitial atoms, r_i^k is the i th component of the equilibrium position of the k th atom in the cell including the interstitial, and $r_i^{\text{interstitial}}$ is the i th component of the position of the interstitial. Using Eq. (2), the elastic dipole tensors for octahedral and hexahedral interstitial oxygen atoms in titanium were calculated (in eV):

$$\mathbf{P}_{\text{oct}} = \begin{bmatrix} 2.71 & 0 & 0 \\ 0 & 2.71 & 0 \\ 0 & 0 & 5.72 \end{bmatrix}, \quad (3)$$

$$\mathbf{P}_{\text{hex}} = \begin{bmatrix} 12.48 & 0 & 0 \\ 0 & 12.48 & 0 \\ 0 & 0 & 4.19 \end{bmatrix}. \quad (4)$$

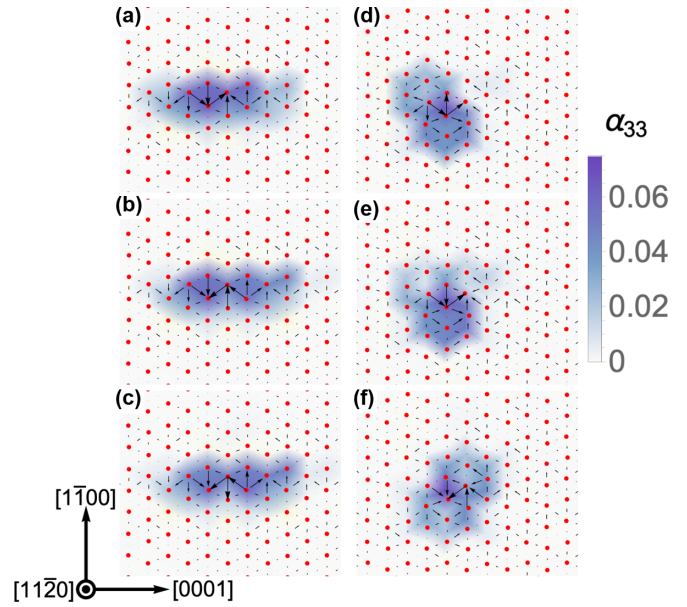


FIG. 2. The screw component of the Nye tensor and the differential displacement map are displayed to show the dislocation spreading in the absence of oxygen. (a)–(c) show the nonstressed prismatic core as it goes from (a) the low energy state to (b) the high energy state to (c) the low energy state on the other side. (d)–(f) show the Schmid-stressed pyramidal core as it goes from (d) low energy state to (e) the high energy contracted state to (f) the low energy state. Note that the slip distance in going from (a)–(c) and (d)–(f) is $c/2$.

As there is no off-diagonal component for either the octahedral or hexahedral oxygen, there is no elastic interaction between these defects and an ideal Volterra screw dislocation. However, as shown in Fig. 2, there is significant spreading of these dislocation cores, and thus, there may be tensile components of the core fields that would interact with the interstitial atoms. To account for these core fields, the strain fields used in the micromechanics calculation are taken from the atomic positions of dislocated cells after their potential energy is minimized.

For the calculation of the strain field around the dislocation, dislocated cells with the same arrangement as those for the NEB calculations were used. For these calculations no oxygen was present, and the length and height of the cell were doubled. The extra width and height were used so that the long-range nature of the interaction between the dislocations and the interstitial atoms could be visualized without significant overlap of the dislocation strain fields. The cells used were $1b$ deep. The strain in the dislocated cells after relaxation was calculated using an edited version of the atomic strain modifier in OVITO [31,32]. This uses a least-squares approach to calculating the deformation gradient \mathbf{F} . With \mathbf{d}_{ji}^0 being the displacement vector between the j th atom and i th atom within some cutoff distance from the i th atom in the reference frame and \mathbf{d}_{ji} being the same in the current frame, \mathbf{F} may be written as

$$\mathbf{F}_i^t = \left(\sum \mathbf{d}_{ji}^{0r} \mathbf{d}_{ji}^0 \right)^{-1} \left[\sum \mathbf{d}_{ji}^{0r} (\mathbf{d}_{ji} - \mathbf{m}_{ij}) \right] \quad (5)$$

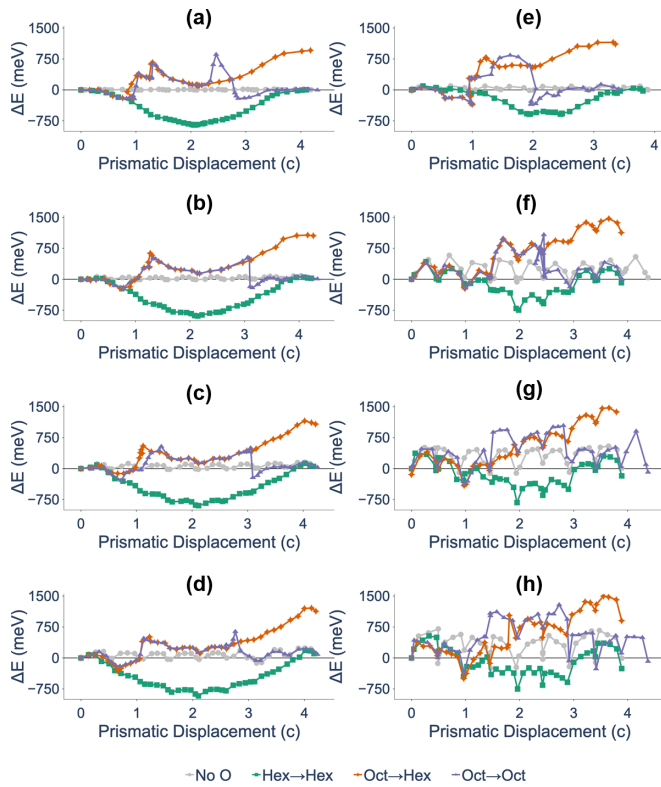


FIG. 3. Relative energy along the NEB pathway for four slip events with and without interstitial atoms. (a)–(d) are under no non-Schmid stress with simulation cells $3b$, $15b$, $30b$, and $60b$ deep, respectively. (e)–(h) are under 3 GPa non-Schmid stress with simulation cells $3b$, $15b$, $30b$, and $60b$, respectively.

The term \mathbf{m}_{ij} ,

$$\mathbf{m}_{ij} = n \text{int} \left(\frac{\mathbf{d}_{ij} - \mathbf{d}_{ij}^0}{|\mathbf{b}|} \right) \mathbf{b}, \quad (6)$$

has been added to the original equation in Ref. [31] and acts to remove the shifts of a full Burgers' vector from the calculation of the deformation gradient. Because the strain calculated this way is based on atomic positions from simulation, it contains nonshear terms that may interact elastically with a point source of dilation.

III. RESULTS

A. NEB of eight slip events

The NEB simulations of eight slip events at distance $c/2$ along the prism plane, which begin $2c$ from the interstitial site and end $2c$ away on the other side, show several interesting features. As seen in Fig. 3, the hexahedral oxygen has an attractive interaction with the dislocation that extends over a medium long range—at least 10 \AA . This attraction is stronger for the prismatic core than for the pyramidal core.

The octahedral oxygen primarily has a repulsive interaction with the dislocation for both the prismatic and the pyramidal spread dislocations, qualitatively matching DFT predictions [33]. However, there is a site adjacent to the dislocation core where there is an attraction between the interstitial and the dislocation which is shown in Fig. 4. This attractive site exists for

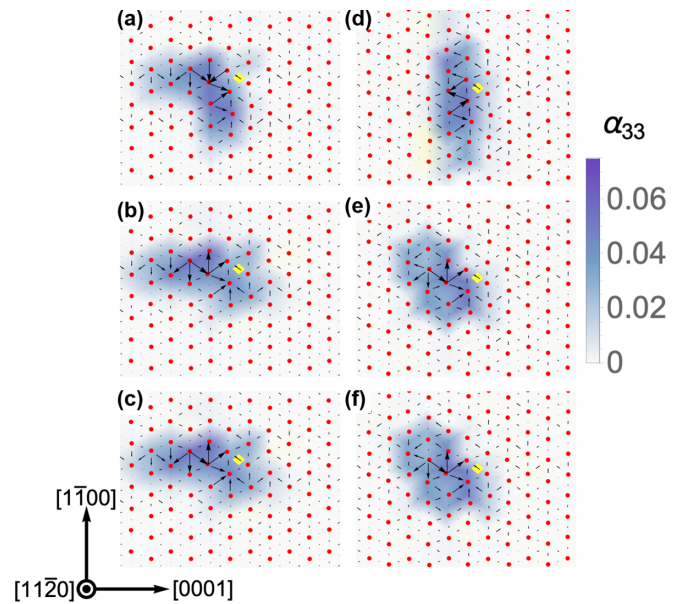


FIG. 4. Nye tensor and Vitek maps of dislocation at the lowest energy metastable core structure seen as the dislocation approaches the octahedral oxygen (where slip number = 1 in Fig. 3). (a)–(c) show the unstressed core for cells that are $3b$, $15b$, and $30b$ thick, respectively. (d)–(f) show the Schmid-stressed core for cells of $3b$, $15b$, and $30b$, respectively. The yellow diamond indicates the position of the oxygen atom.

both core structures and comes with significant rearrangement of the core structure at high oxygen density along the line. Where the interaction is stronger, under non-Schmid stress, there is basal spreading of the dislocation in the $3b$ deep case and pyramidal spreading in the longer cells. In the unstressed case a more complicated core structure is seen instead [see Fig. 4(a)]. However, further studies are necessary to understand the origin of this interaction. One should note that there is a severe underestimate of the basal stacking fault energy in this MEAM potential (170 mJ/m^2 compared to 300 mJ/m^2 in DFT) [34], and it is unclear from these results whether this effect is likely outside of MEAM simulations.

These attractions change the relative energies of the hexahedral and octahedral interstitial atoms as the dislocation approaches. This is shown in Table I, where the far-field values refer to the energy of the interstitial in a nondislocated cell, the adjacent Oct site is the octahedral site directly adjacent to the dislocation core in the slip plane, and the core site is when the oxygen sits in the site within the dislocation core. Note that

TABLE I. Relative energies (in eV) of the various interstitial sites for conditions under which differing cores are stable. The calculations in the prismatic core have no stress applied to the cell. For the pyramidal core, a compressive stress of 3 GPa is applied along the $[1\bar{1}00]$ direction. Values in each row are measured relative to the energy of the far-field octahedral interstitial site.

Core	Far-field Oct	Far-field Hex	Adjacent Oct	Core site
Prism	0	1.20	−0.2	0.16
Pyramidal	0	1.26	−0.15	0.54

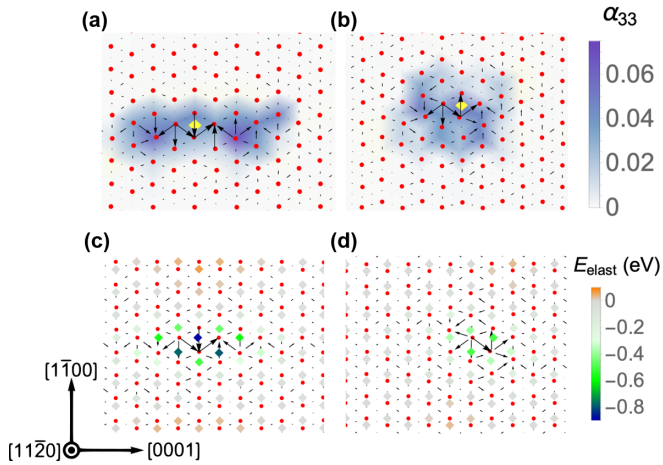


FIG. 5. (a) and (b) show the spreading of the dislocation with the oxygen in the core interstitial site (a) in the unstressed case and (b) with non-Schmid stress applied. (c) and (d) show the calculated elastic interaction from 1 for the prismatic core and hexahedral oxygen and for the pyramidal core and hexahedral oxygen, respectively.

the values in Table I are measured relative to the energy of an oxygen atom at the Oct site in a dislocation-free crystal. In the case of the prismatic core, the chosen cell is stress free. In the case of the pyramidal dislocation core, the reference cell has the 3 GPa non-Schmid stress applied. From the far-field calculation, the application of the non-Schmid stress increases the relative energy of the oxygen at the Hex site by 60 meV. In comparison, the energy of an oxygen atom at the core site increases by 380 meV in the pyramidal core vs the prism.

In both cases, when the dislocation pushes the oxygen into the core interstitial site, it becomes prismatically spread, as shown in Fig. 5(a). The prismatic spread is more pronounced in the absence of non-Schmid stress as can be seen by comparing Figs. 5(a) and 5(b).

Examination of the prismatic core shows that the dislocation remains unkinked, even in the $60b$ deep cells, the largest considered here. In contrast, the pyramidal cores remained straight only in the $3b$ and $15b$ cases, whereas the deeper cells displayed the formation of kinks.

B. NEB of return paths

The NEB paths identified above for the case of shuffling from the octahedral to hexahedral site necessarily show a net increase in energy because the energy of the interstitial atom itself is increased. Although the hexahedral site is higher in energy, the barrier to return to the octahedral site away from the dislocation is non-negligible (0.85 eV according to DFT calculations [35]), so at an appropriate strain rate, if oxygen is shuffled by the dislocation, it may remain in that site long enough for the next dislocation to encounter it.

However, the barrier to return to the lower energy octahedral site within the dislocation core may be lower depending on the dislocation core structure. To assess this barrier, CI-NEB simulations were performed starting from positions along the NEB pathway where the oxygen atom starts in the octahedral site and ends in the hexahedral site and ending at two positions along the NEB pathway where the oxygen

starts and ends in the octahedral site. These simulations were performed using cells $15b$ deep, as that was the deepest simulation cell without significant bowing or kink formation in the pyramidal dislocations in the absence of oxygen and therefore represents how a straight segment of a dislocation would interact with the interstitial obstacle.

In addition, these calculations were repeated with cells under shear (Schmid) stress. Peierls stresses τ_p were roughly estimated from the original NEB calculations without oxygen by using the greatest increase in energy during the slip event when the dislocations were closest to a perfect quadrupolar arrangement and the formula

$$\tau_p = \frac{\Delta E}{\Delta u b^2}, \quad (7)$$

where ΔE , Δu , and b are the change in energy, change in position, and magnitude of Burger's vector, respectively. The Peierls barrier for the prismatic core was estimated to be 40 MPa, and that for the pyramidal core was estimated to be around 200 MPa. NEB simulations for the return paths were repeated at half of the estimated Peierls barrier, 20 and 100 MPa, respectively, for the prismatic and pyramidal cores.

Because the interaction with the octahedral oxygen is a short-range contact interaction, it was expected to be unaffected by the added shear strain, whereas the barrier to motion from the long-range attraction to the oxygen in the hexahedral and core site was expected to be counteracted by the added shear.

The results shown in Fig. 6 show a pronounced barrier to return to the octahedral site for the prismatic core simulation. However, in the pyramidal core simulation there is little to no barrier for return to the octahedral site; this suggests that interstitial shuffling is unlikely to occur when the dislocation is pyramidally dissociated or when it is compact when the oxygen is in the core interstitial site.

C. Micromechanics calculations

The long-range attractive interaction between hexahedral oxygen and the prism core seems well predicted by the micromechanical calculation shown in Fig. 5. As seen in Table I, our MEAM calculations show an attraction between the hexahedral oxygen and the dislocation with a strength of 1.04 eV (0.72 eV) for the prismatic (pyramidal) core. The micromechanical calculation here predicts the hexahedral interstitial has a -0.90 eV (-0.50 eV) attraction to a dislocation in the prismatic (pyramidal) configuration. The values for the prismatic core are in reasonable agreement with the MEAM calculation. For the pyramidal core, the larger energy between the MEAM and micromechanical calculation is unsurprising given the rearrangement in the core structures seen in Fig. 5.

IV. DISCUSSION AND SUMMARY

The first result of this work is stronger evidence for the occurrence of interstitial shuffling of oxygen in α -Ti. Previous work claimed interstitial shuffling could cause slip-plane softening, which is a precursor to brittle failure [5]. Those results relied on GSF calculations as an argument for interstitial shuffling to occur. Using full dislocations instead of stacking faults removes arbitrary constraints on the motion of the interstitial

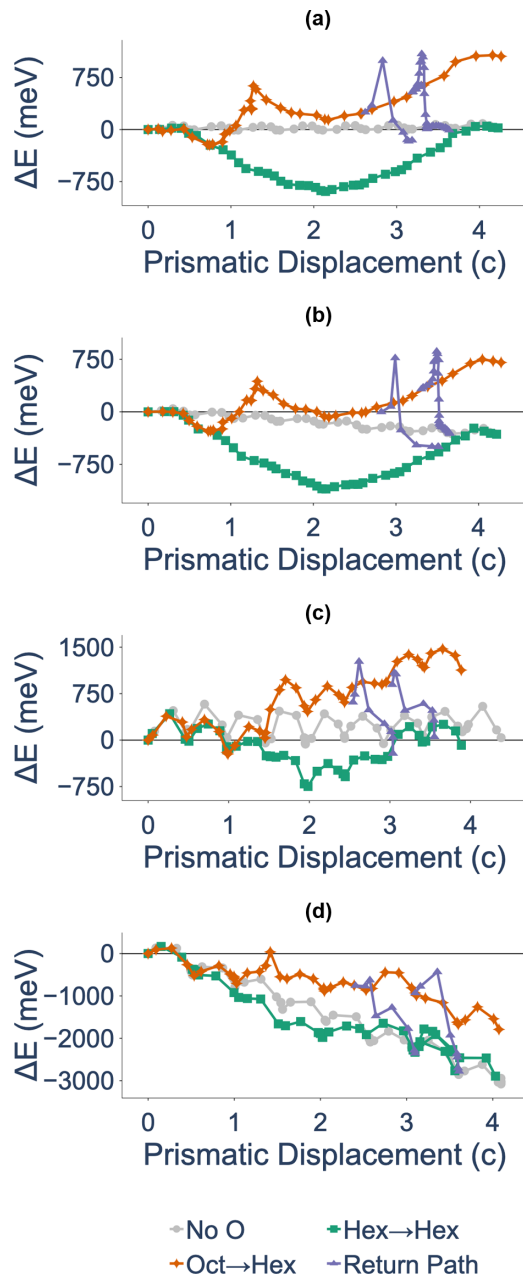


FIG. 6. Relative energy along NEB pathway for four slip events with and without interstitial atoms for the following cases: (a) no non-Schmid or Schmid stress, (b) no non-Schmid stress but shear stress of 20 MPa applied, (c) non-Schmid stressed but unsheared, (d) non-Schmid stressed and shear stress of 100 MPa applied.

as well as Ti atoms in the dislocation core. This in turn enables the interstitial atom to interact with the strain field around the dislocation.

The results presented here show that shuffling is likely to occur given a prismatically spread dislocation core, the preferred core structure under no non-Schmid stress in the MEAM potential used. While the pyramidal core is favored in DFT simulations without oxygen present, the metastable prismatic core is expected when slip is occurring on the prismatic plane [9].

However, the results presented here also show shuffling will be suppressed by an applied non-Schmid stress. Under

TABLE II. Behavior (shuffle or cross slip) of the dislocation encountering oxygen in MD simulations at various strain rates.

$\dot{\epsilon}$	5×10^9	1×10^9	5×10^8	1×10^8
Prism	Shuffle	Cross	Shuffle	Shuffle
Pyramidal	Cross	Cross	Cross	Cross

non-Schmid stress, the core structure is altered to be more pyramidal and remains relatively compact on the prismatic plane even when the dislocation is prismatically slipping. This shows that there is a significant effect of the core structure on dislocation interstitial interaction.

The effect of core structure on the occurrence of shuffling is explained by the difference in attraction between the interstitial oxygen and the core fields of the two dislocation structures, calculated using micromechanics. While the strain field around an idealized screw dislocation is purely shear and therefore would not be expected to interact with the interstitial atom, the core fields around the dislocations in these simulations have tensile components.

The connection between core structure and interstitial shuffling suggests that an alloy which strongly favors the pyramidal core over the prismatic core may have reduced susceptibility to oxygen embrittlement. This may help explain the experimentally observed reduction in oxygen sensitivity seen experimentally in experiments with Ti-xAl alloys [36]. This correlates well with DFT simulations that have shown a propensity for basal and pyramidal spreading of the dislocation core, as well as an increase in the prismatic stacking fault energy [11,37]. As there is interest in discovering more oxygen tolerant Ti alloys, simulation of the dislocation core structure may be a useful step in alloy design.

ACKNOWLEDGMENT

This research was funded by the U.S. Office of Naval Research under Grant No. N0014-19-1-2376.

APPENDIX: MOLECULAR DYNAMICS SIMULATIONS

MD simulations of a dislocation slipping past an octahedral interstitial were performed to examine the possibility of interstitial shuffling at temperature (300 K) and high strain rate. In these simulations the same supercell arrangement as for the 15b cells for NEB were used, but with one octahedral oxygen placed $2c$ away from the left dislocation in the prism direction and six oxygens placed $2c$ from the right dislocation in the prism direction at the same y position as the dislocation and $\pm 1(1\bar{1}00)$ away from the dislocation evenly spaced along the dislocation line. This oxygen served to completely lock the right dislocation so that it did not affect the slip of the left dislocation.

After the cells were equilibrated with one thousand 0.001 ps time steps using a Nosé-Hoover NPT thermostat [38–40] and the Parrinello-Rahman method [41], a constant engineering strain rate oriented for prism slip was applied. MD under the applied strain rate used an NVT SLLOD thermostat [42].

The results under various strain rates and non-Schmid stresses are summarized in Table II.

These results show that the dislocation shuffling an interstitial atom is a possible alternative to cross slip for the prismatic dislocation and that the probability of shuffling may be reduced by application of non-Schmid stress. These results are rather limited as only extremely high

strain rates are examined due to computational limitations on simulation length (for reference, the highest strain rate simulation used in experiments in Ref. [5] was $10^3/s$), and only one simple arrangement of oxygen interstitials was used.

-
- [1] B. Hurlless and F. Froes, *AMPTIAC Q.* **6**, 3 (2002).
- [2] R. Jaffee, *JOM* **2**, 1261 (1950).
- [3] H. Conrad, *Prog. Mater. Sci.* **26**, 123 (1981).
- [4] Q. Yu, L. Qi, T. Tsuru, R. Traylor, D. Rugg, J. W. Morris, Jr., M. Asta, D. C. Chrzan, and A. M. Minor, *Science* **347**, 635 (2015).
- [5] Y. Chong, M. Poschmann, R. Zhang, S. Zhao, M. S. Hooshmand, E. Rothchild, D. L. Olmsted, J. W. Morris, D. C. Chrzan, M. Asta, and A. M. Minor, *Sci. Adv.* **6**, 1 (2020).
- [6] J. Williams, A. W. Sommer, and P. P. Tung, *Metall. Mater. Trans. B* **3**, 2979 (1972).
- [7] V. Gerold and H. P. Karnthaler, *Acta Metall.* **37**, 2177 (1989).
- [8] K. Wolf, H. J. Gudladt, H. A. Calderon, and G. Kostorz, *Acta Metall. Mater.* **42**, 3759 (1994).
- [9] E. Clouet, D. Caillard, N. Chaari, F. Onimus, and D. Rodney, *Nat. Mater.* **14**, 931 (2015).
- [10] M. Poschmann, M. Asta, and D. C. Chrzan, *Modell. Simul. Mater. Sci. Eng.* **26**, 014003 (2018).
- [11] T. Tsuru, M. Itakura, M. Yamaguchi, C. Watanabe, and H. Miura, *Comput. Mater. Sci.* **203**, 111081 (2022).
- [12] M. Poschmann, I. S. Winter, M. Asta, and D. C. Chrzan, *Phys. Rev. Materials* **6**, 013603 (2022).
- [13] D. C. Chrzan, M. Poschmann, I. S. Winter, and M. Asta, *Phys. Rev. Materials* **6**, 013604 (2022).
- [14] P. Zhang and D. R. Trinkle, *Comput. Mater. Sci.* **124**, 204 (2016).
- [15] M. Poschmann, M. Asta, and D. Chrzan, *Comput. Mater. Sci.* **161**, 261 (2019).
- [16] M. S. Daw, *Comput. Mater. Sci.* **38**, 293 (2006).
- [17] N. Lehto and S. Öberg, *Phys. Rev. Lett.* **80**, 5568 (1998).
- [18] E. Clouet, *Phys. Rev. B* **86**, 144104 (2012).
- [19] A. P. Thompson, H. M. Aktulga, R. Berger, D. S. Bolintineanu, W. M. Brown, P. S. Crozier, P. J. in t Veld, A. Kohlmeyer, S. G. Moore, T. D. Nguyen, R. Shan, M. J. Stevens, J. Tranchida, C. Trott, and S. J. Plimpton, *Comp. Phys. Comm.* **271**, 108171 (2022).
- [20] G. Henkelman and H. Jónsson, *J. Chem. Phys.* **113**, 9978 (2000).
- [21] G. Henkelman, B. P. Uberuaga, and H. Jónsson, *J. Chem. Phys.* **113**, 9901 (2000).
- [22] A. Nakano, *Comput. Phys. Commun.* **178**, 280 (2008).
- [23] E. Maras, O. Trushin, A. Stukowski, T. Ala-Nissila, and H. Jónsson, *Comput. Phys. Commun.* **205**, 13 (2016).
- [24] R. Gröger and V. Vitek, *Modell. Simul. Mater. Sci. Eng.* **20**, 035019 (2012).
- [25] C. S. Hartley and Y. Mishin, *Mater. Sci. Eng. A* **400–401**, 18 (2005).
- [26] E. Clouet, L. Ventelon, and F. Willaime, *Phys. Rev. Lett.* **102**, 055502 (2009).
- [27] L. Bai and D. Breen, *J. Graphics Tools* **13**, 53 (2008).
- [28] R. Siems, *Phys. Status Solidi B* **30**, 645 (1968).
- [29] M. Poschmann, Atomistic simulations of screw dislocations in titanium, Ph.D. thesis, University of California, Berkeley, 2018.
- [30] E. Hayward, C. Deo, B. P. Uberuaga, and C. N. Tomé, *Philos. Mag.* **92**, 2759 (2012).
- [31] M. L. Falk and J. S. Langer, *Phys. Rev. E* **57**, 7192 (1998).
- [32] A. Stukowski, *Modell. Simul. Mater. Sci. Eng.* **18**, 015012 (2010).
- [33] N. Chaari, D. Rodney, and E. Clouet, *Scr. Mater.* **162**, 200 (2019).
- [34] R. G. Hennig, T. J. Lenosky, D. R. Trinkle, S. P. Rudin, and J. W. Wilkins, *Phys. Rev. B* **78**, 054121 (2008).
- [35] H. H. Wu and D. R. Trinkle, *Phys. Rev. Lett.* **107**, 045504 (2011).
- [36] Y. Chong, R. Zhang, M. S. Hooshmand, S. Zhao, D. C. Chrzan, M. Asta, J. W. Morris, Jr., and A. M. Minor, *Nat. Commun.* **12**, 6158 (2021).
- [37] P. Kwasniak, H. Garbacz, and K. J. Kurzydowski, *Acta Mater.* **102**, 304 (2016).
- [38] S. Nosé, *Mol. Phys.* **52**, 255 (1984).
- [39] S. Nosé, *J. Chem. Phys.* **81**, 511 (1984).
- [40] W. G. Hoover, *Phys. Rev. A* **31**, 1695 (1985).
- [41] M. Parrinello and A. Rahman, *J. Appl. Phys.* **52**, 7182 (1981).
- [42] B. J. Edwards, C. Baig, and D. J. Keffer, *J. Chem. Phys.* **124**, 194104 (2006).